Journal of Aerosol Science 92 (2016) 38–52

Contents lists available at ScienceDirect

Journal of Aerosol Science

journal homepage: www.elsevier.com/locate/jaerosci

Performance comparison of two thermodenuders in Volatility Tandem DMA measurements

Luís Mendes [a,b], Konstantinos Eleftheriadis [a,*], George Biskos [c,d]

[a] Institute of Nuclear & Radiological Sciences & Technology, Energy & Safety, Environmental Radioactivity Laboratory, N.C.S.R. "Demokritos", Aghia Paraskevi, 15310 Athens, Greece
[b] University of the Aegean, Department of Environment, 81100 Mytilene, Greece
[c] Faculty of Civil Engineering and Geosciences, Delft University of Technology, 2628 CN Delft, The Netherlands
[d] Energy Environment and Water Research Center, The Cyprus Institute, 2121 Nicosia, Cyprus

ARTICLE INFO

Article history:
Received 30 July 2015
Received in revised form
9 October 2015
Accepted 14 October 2015
Available online 22 October 2015

Keywords:
Aerosol volatility
Nanoparticles
Thermodenuder
VTDMA

ABSTRACT

Volatility Tandem Differential Mobility Analysers (VTDMAs) are widely used for determining the volatile and refractory fractions and thus the mixing state of aerosols particles. A three-channel VTDMA consisting of two thermodenuders (TDs) with distinct designs (i.e., the NanoTD, having a straight tube design, and a coiled TD; cTD) and a by-pass line was built and fully characterized. Both TDs were tested using laboratory-generated aerosol particles (single compound and core–shell particles) as well as atmospheric aerosols observed at an urban background station. The NanoTD exhibited high particle penetration efficiency and negligible thermophoretic losses, making it advantageous for ultrafine particle analysis, especially in environments with low particle concentration. The cTD allows longer particle residence time for the same flow rate, resulting in higher particle volatilization in some cases. Higher particle losses in this TD, both thermophoretic and diffusional, pose a limitation when dealing with low particle concentrations.

The difference in the performance between the thermodenuders was only noticed at intermediate temperatures, at which particle volume loss becomes more pronounced. These temperatures vary among aerosols, since the volatilization rate depends on the chemical complexity and size of the particles sampled. Differences in the aerosol volume fraction remaining after heating with the two TD designs exhibited a maximum of 20% for single-compound particles and 12% for urban background aerosols. Measurements using core–shell particles yielded differences of up to 21% in particle volatilization, independently of particle size, when comparing the system using either of the two TD designs. Similar results were obtained with the two TD designs at higher operating temperatures (e.g., 230 °C), indicating that at this temperature most of the material on the particles was evaporated.

1. Introduction

Atmospheric aerosol particles can affect the climate of the Earth by directly absorbing and scattering radiation, or indirectly by acting as cloud condensation nuclei (CCN) (IPCC, 2007; Lohmann and Feichter, 2004). At the same time, they pose a great risk on humans due to their adverse health effects (Colome, Kado, Jaques, & Kleinman, 1992; Cullen et al., 2000;

* Corresponding author.
E-mail address: eleftheriadis@ipta.demokritos.gr (K. Eleftheriadis).

http://dx.doi.org/10.1016/j.jaerosci.2015.10.002

Davidson, Phalen, & Solomon, 2005; Oberdörster et al., 2004; Pope, 2000). High concentrations of ultrafine particles (UFPs, i.e., particles having diameters smaller than 100 nm) have been shown to correlate well with hospital readmission of patients (Von Klot et al., 2005) and human health effects by several epidemiological studies (Donaldson et al., 2002; Li et al., 2003; MacNee, & Donaldson, 2003). UFP can also act as particle bound mutagens carriers to the lung (Kawanaka, Matsumoto, Sakamoto, & Yun, 2011). Due to their small diameter, ultrafine particles have the ability to penetrate deep into the lungs and reach the alveolar region (ICRP, 1995). Nevertheless, it is not clear which chemical or physical–morphological properties of particles are responsible for the adverse health effects (Harrison & Yin, 2000).

The low mass concentration, short life-time and complex composition of UFPs typically observed in the environment makes traditional filter sampling and offline analysis methods unsuitable when high time resolution measurements are required. Tandem Differential Mobility Analyser systems, introduced by Liu et al. (1978) and adapted to study several intrinsic particle properties like hygroscopicity volatility and organic content (Rader and McMurry, 1986), provide an effective alternative analysis technique.

Volatility is increasingly considered one important property to assess both in short-term campaigns and long-term routine measurements in air quality stations (Poulain et al., 2014). The study of aerosol volatility can provide valuable real-time information on particle mixing state, which can be used to indirectly infer their chemical composition (An, Pathak, Lee, & Pandis, 2007; Burtscher et al., 2001; Jennings, O'Dowd, Cooke, Sheridan, & Cachier, 1994; Kuhn, Biswas, Fine, Geller, & Sioutas, 2005; Orsini et al., 1999; Philippin, Wiedensohler, & Stratmann, 2004; Poulain et al., 2014; Sakurai, Park, Mcmurry, & Kittelson, 2003). VTDMA measurements have been used to determine the volatility of particles observed in the atmosphere (Burtscher et al., 2001; Engler et al., 2007; Frey et al., 2008; Kuhn, Biswas, Fine, et al., 2005; Kuhn, Biswas, Sioutas, 2005; Moore, Ning, Ntziachristos, Schauer, & Sioutas, 2007; Philippin et al., 2004; Tiitta et al., 2010; Wehner, Philippin, Wiedensohler, Scheer, & Vogt, 2004) and synthesized in the laboratory (An et al., 2007; Johnson, Ristovski, & Morawska, 2004; Maruf Hossain et al., 2012; Orsini et al., 1999; Paulsen, Weingartner, Rami Alfarra, & Baltensperger, 2006; Villani, Picard, Marchand, & Laj, 2007), while recently developed miniaturized, lightweight and cost-effective classifiers (cf. Bezantakos et al., 2015) can further reduce their complexity and increase their portability.

The operating principle of the VTDMA is rather simple: one DMA is used to select from the polydisperse aerosol sample particles that have sizes within a very narrow range (i.e., monodisperse aerosol), which are then passed through a thermodenuder (TD) maintained at a certain temperature. Some volatile components volatilize and are removed from the flow by desorption. The resulting particle size distribution after heating is analyzed using a second DMA coupled with a Condensation Particle Counter (CPC). The volatilized and remaining (refractory) aerosol fractions are usually expressed in terms of number, mass or volume of particles.

Several TD designs have been developed and used in different instrument setups. Particle volatilization inside the thermodenuder has been shown to depend on several factors. Cappa (2010) and Riipinen, Pierce, Donahue, and Pandis (2010) argued that evaporation kinetics models are essential to interpret thermodenuder measurements, suggesting that the equilibrium inside a TD cannot be reached at any reasonable particle residence time for common laboratory or ambient aerosols. Saleh, Shihadeh, and Khlystov (2011) concluded that equilibration kinetics in a TD are not affected by volatility, but instead by the aerosol particle size and number concentration, evaporation coefficient, and vapour diffusivity. Karnezi, Riipinen, and Pandis (2014) pointed out the role of vaporization enthalpy and potential mass transfer resistances as particles evaporate.

The inclusion of a desorption section aiming to reduce vapour re-condensation has been adopted in several TD designs (An et al., 2007; Faulhaber et al., 2009; Fierz, Vernooij, & Burtscher, 2007; Huffman et al., 2009). Cappa (2010) also acknowledged the role of this section in his kinetic model. Saleh et al. (2011) proposed guidelines for TD design without desorber, arguing that the re-condensation is not significant in laboratory or ambient TD measurements.

Due to the complexity in describing particle behavior inside TDs, there is a need to further study their performance and the influence of their design.

This work intends to characterize and compare two thermodenuder designs, using a VTDMA system developed to perform volatility measurements of fine and UFP. To do so, we assess the performance of both TDs designs by employing them within the VTDMA system using several laboratory-generated aerosols, as well as atmospheric aerosols. Both TDs consist of a heater and a desorption section, however their geometry is rather distinct, affecting especially the particle residence time in the heating tube and the temperature profile in the cooling section. The side by side comparison of the TDs allows to experimentally evaluate influence of their design in the particle penetration efficiency and volatilization performance, using similar aerosol. The influence of particle size is also considered.

The experimental results of this study provide an indication of how comparable volatility studies are, and how TDs perform differently depending on the complexity of the aerosol studied.

2. Material and methods

2.1. Description of the VTDMA set-up

Fig. 1 shows a schematic layout of the entire VTDMA system used in this study. The system consist of a radioactive aerosol neutralizer for applying a well-defined charge distribution to the particles, a first DMA (DMA-1) for selecting particles having electrical mobilities within a very narrow range, a thermodenuder for heating the monodisperse aerosol and a

second DMA (DMA-2) coupled with a CPC for measuring the size distribution of the conditioned aerosol. Three-way valves placed downstream the aerosol neutralizer allow bypassing DMA-1 for polydisperse aerosol analysis, or the entire conditioning system, thereby operating the entire setup as a Scanning Mobility Particle Sizer (SMPS).

Both DMAs were operated at an aerosol flow of 0.3 L min^{-1}, controlled by the CPC (TSI Model 3022A). The sheath flow was set to 1.5 L min^{-1} in DMA-1 and 3 L min^{-1} in DMA-2, using custom-made glass critical orifices. The flows of the DMAs were calibrated using a bubble flow meter (Gilibrator-2) and the inner rod voltage was verified with a multimeter before the measurements. The performance of the system was checked using PSL spheres of four standard diameters (90, 173, 200 and 262 nm), confirming the expected particle size accuracy within 3%.

The sheath flow systems are arranged in independent closed loops, incorporating filters (PALL Corporation, part number 12144), a silica gel dryer (volume of 1 L), a diaphragm pump (Vacuubrand GmbH, model MD-1) and a buffer box for flow and temperature stabilization. This setup provides robust, stable and accurate flows to the instrument (Jokinen and Mfikelfi, 1997; Taylor, 2007). The closed loop arrangement allows also a longer operation time of the dryers, since the only entry point of the vapour in the system is from the aerosol flow.

The system includes three operating channels: one bypass channel at ambient temperature and two channels with TD units. The use of multiple TD units allows improved time resolution of the measurements. With a time resolution of one hour one can analyze five particle sizes at two TD temperatures. However, the sampling program is fully customizable to adapt to the objectives of the study, and the TDs may be operated in temperature stepping mode. The parameters describing the thermodenuders are very important in the VTDMA system and are described in detail in Section 2.2.

2.2. Thermodenuders characterization

2.2.1. Thermodenuders design

The NanoTD is a thermodenuder designed for minimizing particle loss and recondensation of the evaporated vapors. The details and a characterization of the NanoTD are provided by Fierz et al. (2007). In brief, the NanoTD has three independent heaters, one for volatilization of the particles, and two located in the adsorption section. The heaters are set for stepwise decreasing temperature, allowing gradual cooling of the flow and adsorption of volatile species in gas-phase to the walls. The volatilization stainless steel tube is 10 cm long and and has a 0.8-cm inner diameter, while the adsorption unit is 20-cm long. The NanoTD can operate at a maximum temperature of 235 °C continuously and 250 °C for short periods.

The custom-made thermodenuder (cTD), shown in Fig. 2, consists of a coiled copper tube (103 cm length, 0.45 cm inner diameter and 0.6 cm outer diameter), heated by a heating tape and thermally insulated with glass wool (Nyeki, Coulson, & Colbeck, 2005). The coil has 5.5 turns and a diameter of 6.0 cm, resulting in a total TD length of 121 cm. The adsorption unit

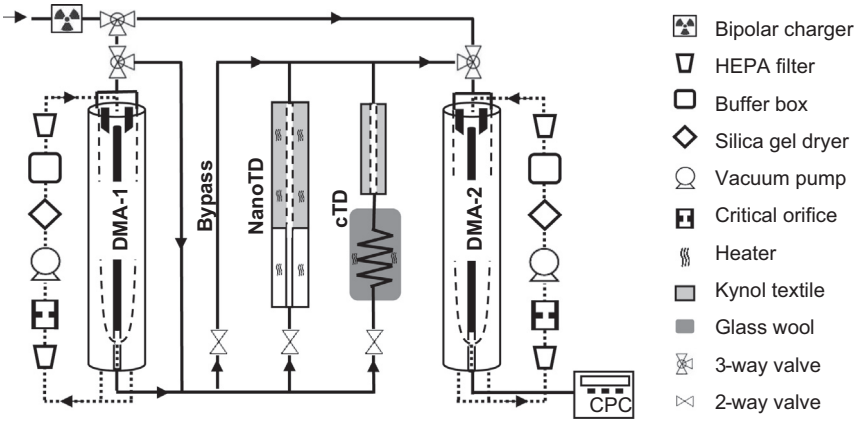

Fig. 1. Schematic diagram of the VTDMA system consisting of two DMAs, two TDs and a CPC.

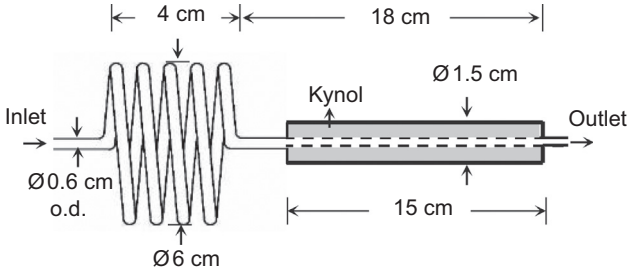

Fig. 2. Diagram of the coiled thermodenuder (cTD) used in this study.

is 15 cm long, and similarly to the NanoTD it consists of a steel mesh tube wrapped in Kynol textile (Kynol Europa GmbH, product ACC-5092-20) and is enclosed in a copper tube with a diameter of 1.5 cm. In this case, the adsorption unit is not heated and the aerosol flow cools down faster while passing through. The temperature is controlled using a thermostat and a thermocouple placed in the center of the coil, achieving an operating temperature of up to 450 ± 2 °C. Applying temperatures higher than 300 °C is likely to carbonise organic compounds inside the tube (Birmili et al., 2010; Poulain et al., 2014), thereby affecting the estimation of the refractory fraction of the aerosol. As a result, 300 °C is considered the maximum operating temperature in this study. The cTD has the advantage of providing high particle residence times in a compact design, adding the enhanced heat tranfer of coiled-tube flows.

The flow temperature and velocity profiles in the TDs were simulated using the non-isothermal laminar flow module of COMSOL Multiphysics software (Version 5.0). The tube walls were set to constant temperature in the heated sections, while the remaining tubes were simulated for heat exchange between the internal wall, the tube walls, and the external environment. The convective heat flux to external environment was adjusted so that the simulated flow temperatures matched the measured temperatures at the outlet. The simulation volume was extended by 10 cm before and after the TD to determine the temperature profile of the aerosol at the inlet and outlet channels. Both TDs were simulated at an operating temperature of 250 °C and the results are shown in Fig. 3. The NanoTD temperature profile is in agreement with a similar simulation performed by Fierz et al. (2007). The temperature profile of the NanoTD tube wall in the three heating sections corresponds to the set temperatures in each heater (i.e., 250/175/100 °C), which for reasons of simplicity were simulated as tubes at constant temperature. The transition between heaters was not considered.

The tube center-line represents the position of the aerosol that will take longer to equalize its temperature with the tube wall.

The radial flow velocity was calculated by COMSOL, taking into account the temperature profiles averaged along the heated section, in order to obtain a representative average flow speed. Fig. 4 shows the estimated residence time in the heated section of each TD as a function of the applied temperature, at a flow rate of 0.3 L min^{-1} (1 atm, 25 °C). The NanoTD has a residence time of 1.0 s at ambient temperature, which is reduced to 0.58 s (i.e., by 42%) at the maximum operating temperature of 250 °C, whereas the cTD exhibits a reduction in residence time from 3.2 s at ambient temperature to 1.79 s (i.e., by 44%) at 250 °C and 1.6 s (i.e., by 50%) at 300 °C.

The volatilization of particles in a thermodenuder is fundamentally determined by the kinetics of the evaporation process (Cappa, 2010), and assuming that equilibrium between the particle and gas-phase is achieved within a few seconds

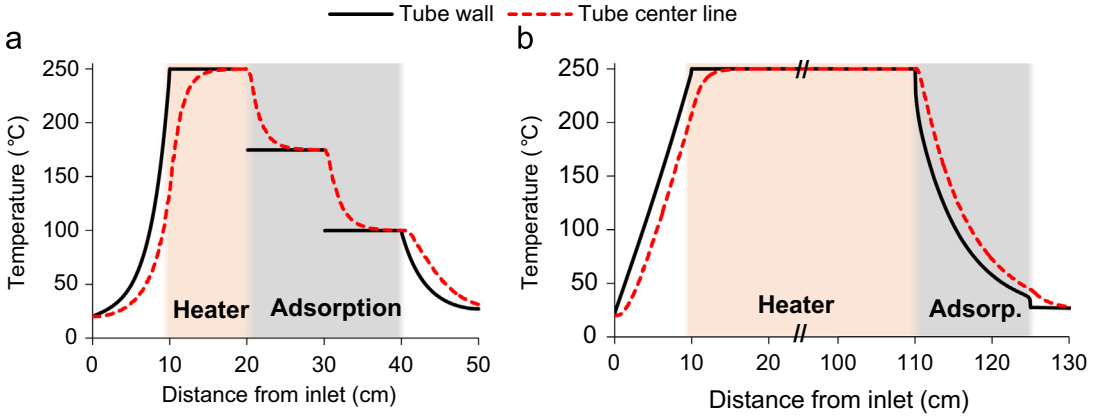

Fig. 3. Simulated temperature profiles of the flow and tube walls of (a) the NanoTD and (b) the cTD, both operated at 250 °C. The main heater and adsorption sections are represented as shadowed areas. The temperature profiles in plot (b) are shortened in the heater section to improve visualization.

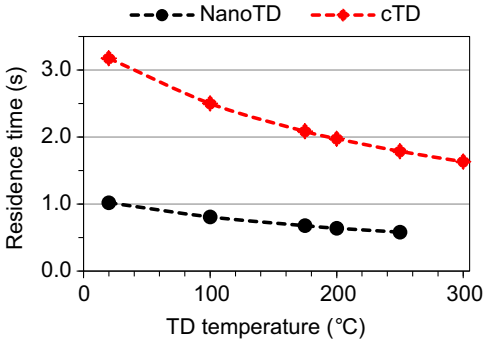

Fig. 4. Aerosol residence time in the heated section of the NanoTD and the cTD, as a function of applied temperature and flow of 0.3 L min^{-1}. The markers represent the temperatures simulated in COMSOL Multiphysics software.

may lead to underestimation of particles volatility (An et al., 2007; Riipinen et al., 2010). For this reason, and due to the sensitivity to the residence time, different TD designs are likely to produce different volatilization rates for the same aerosol.

2.2.2. Theoretical particle penetration efficiency

In this section we resume the theoretical and semi-empirical equations that govern the particle losses inside a tube, which we then use to compare with the experimental results in Section 3.1. The particles can be deposited along the system by diffusion, sedimentation, thermophoresis and electrostatic forces. Since the aim in this study is to focus on particles with mobility diameter (Dp) smaller than 200 nm, sedimentation losses are not considered. All the tubing in the system is electrically conductive in order to minimize electrostatic losses, which were considered negligible. Particle penetration efficiency in the TD units was determined both theoretically and experimentally. Taking diffusion losses into account, the estimated particle penetration efficiency through a straight tube is given by (Hinds, 1999)

$$P_d = 1 - 5.5u^{2/3} + 3.77\mu \quad \text{for} \quad u < 0.009 \tag{1}$$

where u is a dimensionless deposition parameter given by

$$u = D\,L/Q \tag{2}$$

Here D ($m^2\ s^{-1}$) is the diffusion coefficient of the particles, L (m) is the length of the tube and Q ($m^3\ s^{-1}$) is the volumetric flow rate through the tube.

In the case of a coiled tube, which enhances the formation of secondary flows, the particle penetration efficiency ($P_{d,\,coil}$) can be estimated as (Yook and Pui, 2006):

$$P_{d,coil} = \begin{cases} 1 - 2.5104\zeta^{1/3} + 12.9919\zeta^{2/3} - 37.8238\zeta + 32.8761\zeta^{4/3} & \text{for} \quad \zeta < 0.01 \\ 0.5526e^{-3.657\zeta} + 0.2250e^{-22.3\zeta} + 0.0726e^{-57\zeta} & \text{for} \quad 0.01 < \zeta < 0.2 \end{cases} \tag{3}$$

Here ζ is a non-dimensional parameter describing the particle deposition in coils assuming it is a by-product of secondary flow and Brownian diffusion. This parameter is expressed as follows:

$$\zeta = \delta\,D\,t/a^2 \tag{4}$$

with δ represents the boundary layer thickness of the secondary flow normalized by the inner tube radius a (m), and t (s) the flow residence time inside the tube.

At ambient temperature, assuming an isothermal flow and aerosol particles in the UFP size range, we can consider that particle deposition occurs mostly due to Brownian motion. Nonetheless, in a non-isothermal system with relatively cool walls, thermophoresis causes aerosol particles to move towards and deposit on the walls (Housiadas and Drossinos, 2005; Walsh et al., 2006).

A particle tracing simulation was made in COMSOL Multiphysics software, taking into account the Brownian, drag and thermophoretic forces applied to the particles. Fig. 5 illustrates the direction of the thermophoretic force along the different sections of the cTD, corresponding to conditions of heating, constant temperature and cooling, when operating the TD at 300 °C.

As observed in our simulation, in the TD heating section (cf. Fig. 5a), the thermophoretic force will favor the focusing of the particles in the center of the tube, since the tube wall is hotter than the aerosol flow. Once the flow equals the temperature of the tube wall (cf. Fig. 5b), the thermophoretic force ceases to exist. At the exit of the heating section (cf. Fig. 5c), the tube walls cool down faster than the gas, creating a temperature differential that enhances particle deposition.

Several studies have provided semi-empirical and numerical models to predict the thermophoretic deposition efficiency (η_{th}) inside a tube (Batchelor and Shen, 1985; Housiadas and Drossinos, 2005; Lin and Tsai, 2003; Romay, Takagaki, Pui, & Liu, 1998;

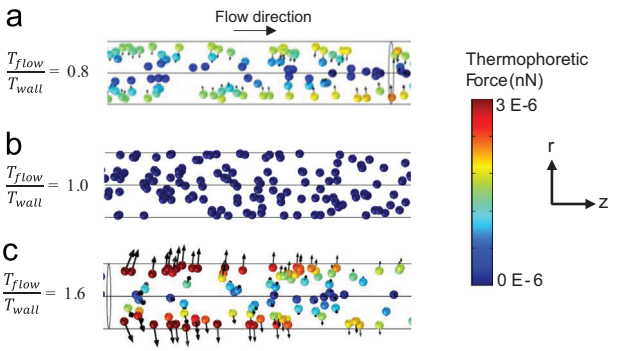

Fig. 5. Simulated thermophoretic forces when particles (a) are heated, (b) reach the tube wall temperature and (c) cool down after leaving the heating section. The color scale indicates the magnitude of the radial thermophoretic force, whereas the arrows on each particle indicate the direction and magnitude of that force. The flow (T_{flow}) and tube wall (T_{wall}) temperatures represent the average values for the domains shown in the figures. (For interpretation of the references to color in this figure legend, the reader is referred to the web version of this article.)

Stratmann, Otto, & Fissan, 1994; Walker, Homsy, & Geyling, 1979). Lin and Tsai (2003) proposed the following semi-empirical equation for laminar flow:

$$\eta_{th} = 0.783\left(Pr\ K_{th}/\theta^*\right)^{0.94} \quad \text{for} \quad 0.007 < Pr\ K < 0.19 \tag{5}$$

and Housiadas and Drossinos (2005) an equation for laminar and turbulent flows based on 1D heat and mass transfer analysis:

$$\eta_{th} = 1 - \left(\theta^*/1+\theta^*\right)^{PrK_{th}} \tag{6}$$

In these models K_{th} represents the thermophoretic coefficient and θ^* the temperature gradient between the wall and gas. In this study, the thermophoretic coefficient was determined according to Talbot, Cheng, Schefer, and Willis (1980). The gas Prandtl number Pr used in Eqs. 5 and 6 is given by

$$Pr = Cp\ \mu/k \tag{7}$$

where Cp represents the specific heat ($J\,kg^{-1}\,K^{-1}$), μ the dynamic viscosity ($N\,s\,m^{-2}$) and k the thermal conductivity ($W\,m^{-1}\,K^{-1}$).

Temperature profiles inside the TDs affect also the diffusion of particles, which should be accounted for determining both the total particle losses required for predicting the penetration efficiency of heated TDs.

2.3. Experimental set-up

2.3.1. Particle generation methods

Aerosol penetration through the TDs was determined experimentally using sodium chloride (NaCl) particles. These particles were produced by atomization (Topas atomizer, Model ATM 221) of a solution with concentration 0.4% (w/v), and dried in a mixing chamber (volume of 100 L), where the aerosol flow ($1\ L\ min^{-1}$)was diluted with dry filtered air (RH < 10%) flow ($10\ L\ min^{-1}$). The solution used in the atomizer was prepared by mixing 0.4 g of NaCl (99.5% purity; MERCK MILIPORE) in 100 ml of purified water (Milli-Q Academic; Millipore).

NaCl particles are non-volatile in the temperature range used in our system (i.e., up to 300 °C), so any particle losses should be attributed to the particle deposition mechanisms described above. The particle size distribution of the aerosol was measured upstream and downstream of each TD in order to determine the particle losses. To account for thermophoretic losses, the size distribution measurements were repeated at different TD temperatures in the range 25–200 °C for the NanoTD, and 25–300 °C for the cTD.

The performance of the TDs was evaluated using laboratory-generated ammonium sulphate particles. The particles were produced from a solution with concentration 0.4% (w/v) by the same method used for the NaCl particles. The expected behavior of ammonium sulphate aerosol particles when heated makes them suitable when evaluating VTDMA systems. The solution used in the atomizer was prepared by mixing 0.4 g of $(NH_4)_2SO_4$ (99% purity; CARLO ERBA REAGENTS) in 100 ml of purified water (Mili-Q Academic: Millipore). Since it is also necessary to evaluate the ability of the system to differentiate non-homogenous aerosol populations as well as core–shell particles from which we can remove their volatile fractions, we also used Di-Ethyl-Hexyl-Sebacat or DEHS ($C_{26}H_{50}O_4$, TOPAS GmbH), which is a long chain volatile compound with high volatilization temperature, to produce volatile aerosol particles.

The use of NaCl particles coated with DEHS provides an internally mixed aerosol of core–shell particles with similar behavior to aged atmospheric aerosols. Monodisperse aerosol particles having diameters of 50 and 100 nm were selected using a mobility classifier (TSI, model 3080). The monodisperse NaCl particles were passed through an Erlenmeyer flask containing DEHS heated at 140 °C. The volatilized DEHS exits the Erlenmeyer flask together with NaCl particles, and condenses on their surface when cooled to ambient temperature, creating coated particles. Fig. 6 illustrates the experimental set-up used for these measurements. The VTDMA, in this particular case, was operated only as a Volatility DMA (VDMA), since DMA-1 was bypassed.

2.3.2. Ambient aerosol experiments

Tests using ambient aerosol particles were performed in order to evaluate and compare the performance of both TD designs in the VTDMA. The tests took place at the "DEM" urban background Global Atmosphere Watch (GAW) Station located at NCSR "DEMOKRITOS", Athens, Greece. Monodisperse aerosol particles with mobility diameters of 30, 50, 80 and 150 nm were selected by DMA-1 and sequentially passed through the TD units and bypass channel, making a cycle of measurements lasting one hour. Both TDs were kept at similar temperatures and at least 30 cycles of measurements were performed for each temperature. The operating temperatures of the TDs ranged between 25 and 230 °C.

2.4. Data treatment methodology

Several approaches have been proposed to process TDMA raw data (Cubison, Coe, & Gysel, 2005; Gysel, Mcfiggans, & Coe, 2009; Stolzenburg & McMurry, 2008). In this study, since the focus is the intercomparison between TD units, a simple approach was taken, similarly to several UFP volatility studies published (Kuhn, Biswas, Fine, et al., 2005; Kuhn, Biswas, Sioutas, 2005; Kuhn, Krudysz, et al., 2005; Moore et al., 2007; Villani et al., 2007).

While DMA-1 was operated at a fixed voltage in order to produce a monodisperse aerosol flow, DMA-2 was operated in scanning mode while the CPC counted the particles concentration for each size bin. When the aerosol passes through the

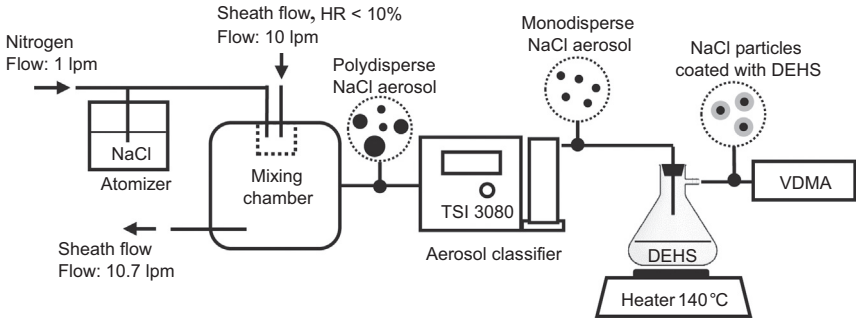

Fig. 6. Schematic diagram of the experimental set-up for producing monodisperse NaCl particles coated with DEHS. The VTDMA system operated as VDMA, bypassing DMA-1.

bypass channel, the measured size distribution corresponds to that of the monodisperse aerosol that exits DMA-1. Similarly, when passing the aerosol trough the TD units, the retrieved size distribution corresponds to the aerosol exiting the TD after conditioning. In both cases the size distribution is corrected for particle losses occurring within the bypass or TD channels. Alternated measurements of bypass and TD channels allow comparison of the aerosol size distribution before and after conditioning. It is assumed that particles keep their charge throughout the system and the influence of multiply charged particles is not considered.

The penetration efficiency η through the TDs, with respect to the bypass channel was calculated as

$$\eta = n_{TD}(T)/\, n_b \tag{8}$$

where $n_{TD}(T)$ is the number of particles passing through the TD set at temperature T (°C), and measured by the CPC downstream DMA-2, while n_b is the measured particle concentration measured when bypassing the TD. Since η depends on particle size, this calculation was repeated for several particle sizes, and the results were fitted with a power-law function given by:

$$\eta = a\, Dp^b + c \tag{9}$$

where Dp is the particle mobility diameter (nm), whereas a, b and c are factors that depend on the TD and the temperature used. The results from these calculations are analyzed in Section 3.1.

Assuming n as the particle number concentration measured for each size bin within upper (u) and lower (l) boundaries, the total number N_T and volume V_T concentrations, as well as the geometric mean diameter M_G measured in the X channel (i.e., TD or bypass) are given by

$$N_{T,X} = \sum_{l}^{u} n/\eta \tag{10}$$

$$V_{T,X} = \sum_{l}^{u} n\pi\, Dp^3/6\eta \tag{11}$$

$$M_{G,X} = \exp\left[\sum_{l}^{u} n \ln Dp^3\ /\eta N_{T,X}\right] \tag{12}$$

The total number and volume measured in the bypass channel or any of the TDs set at ambient temperature should be similar, resulting in remaining number and volume fractions close to one. The number (ΦN) and volume (ΦV) fractions remaining after conditioning at TD temperature T and the shrink factor (SF), are generally used to express the aerosol volatility, and are given by:

$$\Phi N = N_{T,TD}/N_{T,bypass} \tag{13}$$

$$\Phi V = V_{T,TD}/V_{T,bypass} \tag{14}$$

$$SF = M_{G,TD}/M_{G,bypass} \tag{15}$$

Particles shrinking to sizes lower than the detection limit of the instrument will result in the overestimation of the mean size and adulterate the estimated shrink factors.

In order to evaluate the performance of the method described above in comparison with the improved fitting algorithm "TDMAinv" (Gysel et al., 2009), a data set of 73 measurements was compared and the results are shown in Fig. 7. The data refer to measurements using 50- and 150-nm laboratory-generated ammonium sulphate particles produced as described in Section 3.2. The remaining volume fraction obtained with the method applied here is in good agreement with the results

obtained from the TDMAinv method, with an average error of 3%, which is slightly more pronounced for low volume fractions.

3. Results and discussion

3.1. Particle penetration efficiency

In this section we analyze the results obtained for the particle penetration efficiency in both TDs, exploring three major points:

- The experimental determination of particle penetration efficiency through both TDs, at ambient temperature, and comparison with semi-empirical estimations.
- Quantification of the thermophoretic particle deposition in both TDs.
- Verification of the agreement between the observed thermophoretic losses and theoretical predictions.

Fig. 8 shows the measured particle penetration efficiency through the NanoTD (a) and the cTD (b). The theoretical estimation of diffusion losses is also plotted in comparison with experimental results. For the NanoTD this estimation was based on Eq. (1), whereas for the cTD it was based on Eq. (3). Particle losses at 25 °C are considered exclusively diffusional.

Agreement between measurements and predictions at 25 °C is within 1% for the NanoTD in the entire size range investigated in this study (i.e., 13–150 nm). For the cTD, the agreement is within 0.5% for particles smaller than 30 nm, but increases up to 3% for larger particles. The particle penetration efficiency in the NanoTD, ranges between 82 and 99% at

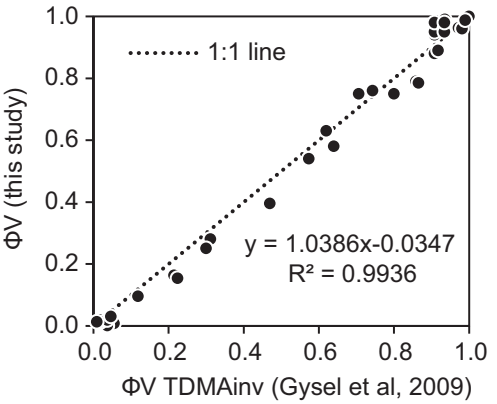

Fig. 7. Comparison between particle volume changes determined by inverting the VTDMA measurements using the method presented in this study and the TDMAinv fitting algorithm provided by Gysel et al. (2009).

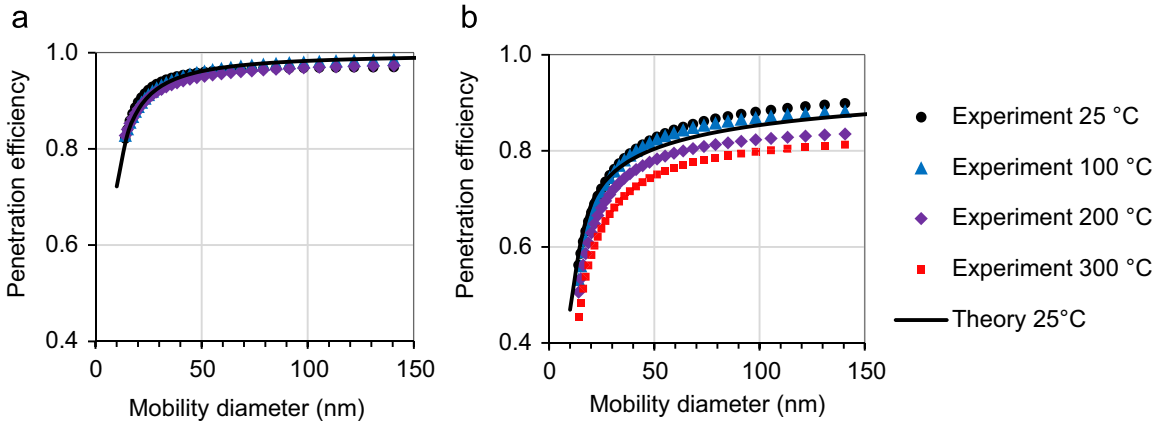

Fig. 8. Particle penetration efficiency between TD inlet and DMA-2 of the (a) NanoTD and (b) cTD. The markers represent fitted experimental data at TD temperatures of 25, 100, 200 and 300 °C. The continuous curves are theoretical calculations of penetration efficiency assuming only diffusion losses at 25 °C.

25 °C, for the particle size range studied here. The cTD exhibits much lower penetration efficiency, ranging between 57 and 87% at 25 °C. This is attributed to the longer volatilization tube and coiled design that enhances the formation of secondary flows.

The NanoTD does not show significant increase in particle losses even at temperatures as high as 200 °C, confirming the results reported by Fierz et al. (2007). The gradual cooling minimizes the thermophoretic force thereby improving the particle penetration efficiency through the TD. The larger tube diameter also allows particles to concentrate further away from the tube walls in the heated section, allowing some radial movement in the cooling section before hitting the walls. On the other hand, the experimental results shown in Fig. 8b indicate that on average particle penetration efficiency in the cTD decreases by 8% at 300 °C. Since the diffusional losses estimated at 300 °C for this TD using Eq. (3) were found to be within 1% of those estimated at 25 °C, we attribute the penetration efficiency reduction to thermophoretic losses only. The results shown here prove that thermophoretic forces can be greatly minimized by improving the TD unit design.

Moving to the third major point of this section, we explore how available numerical models can predict the thermophoretic losses measured in cTD. The NanoTD was not subject to this scrutiny since no significant increase in particle losses was observed when operating it at high temperatures.

The theoretical interpretation of thermophoretic deposition efficiency is not straightforward and requires knowledge of the particle thermal conductivity and a full characterization of the three dimensional (3D) temperature profile inside the TD. Using the flow temperature and velocity profiles simulated as described in Section 2.2.1, as well as the tube wall temperature, we estimated the theoretical thermophoretic losses at 300 °C.

The temperature profile simulation has a maximum amplitude between the wall of the tube and its centreline of about 105 °C, located right after the heated section. With this temperature gradient, the thermophoretic deposition models given by Eqs. (5) and (6) yield mean particle deposition efficiencies of 8.0 and 7.6%, respectively. The results are in good agreement with experimental data, validating the assumption that particle penetration efficiency is reduced mainly by thermophoretic forces.

Since estimating thermophoretic particle deposition requires a large number of input parameters which are often difficult to measure accurately, we consider that the experimental determination of penetration efficiency should be performed when possible.

3.2. Volatilization performance of the thermodenuders

3.2.1. Laboratory tests

Fig. 9 shows the volume thermograms of ammonium sulphate aerosol particles obtained with both TDs. The ability to volatilize ammonium sulphate particles was tested both with monodisperse and polydisperse aerosols. Monodisperse particle sizes having diameters of 50 (cf. Fig. 9a) and 150 nm (cf. b) were used to assess the performance dependence on particle size. The polydisperse aerosol was analyzed when bypassing DMA-1 (cf. Fig. 9c). The geometric mean diameter and geometric standard deviation of the polydisperse size distribution were 48 nm and 1.91, respectively.

The results are expressed in remaining volume fraction (ΦV) and each point represents the average of at least 5 measurements. The monodisperse aerosol volatilization temperatures were generally lower for smaller particles, with the 50-nm particles volatilizing completely at approximately 180 °C, while that happens at 200 °C for the 150-nm particles. In the case of polydisperse aerosols, the volatilization temperature was even higher, with almost full volatilization achieved at around 230 °C. Some remnants were observed even at 300 °C, which can be explained by impurities in the solution that led to the presence of other less volatile components in the resulting particles.

The obtained volatilization temperature of about 230 °C for polydisperse ammonium sulphate particles is within the average range between 180 and 280 °C reported in the literature (Brooks, Smith, Hill, & O'Dowd, 2002; Burtscher et al.,

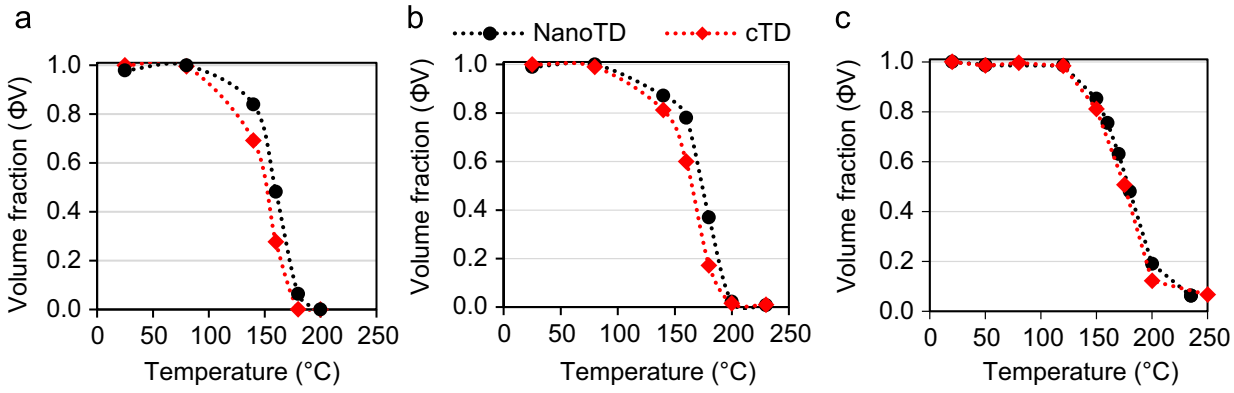

Fig. 9. Volume fraction remaining of ammonium sulphate monodisperse particles with dry diameter of (a) 50 nm and (b) 150 nm, as well as (c) polydisperse particles.

2001; O'Dowd, Jennings, Smith, & Cooke, 1992; Philippin et al., 2004). Lower volatilization temperatures observed for smaller particles (i.e., at 160 and 180 °C for 50- and 150-nm particles, respectively) have also been reported by Villani et al. (2007), highlighting the dependence on particle size.

Comparing TD designs, the NanoTD exhibited significantly lower volatilization of particles in the steeper region of the volatilization curve shown in Fig. 9. The difference in the volume fraction remaining between TDs reaches 20% in the data shown in Fig. 9a and b. The data shown in Fig. 9c indicate a maximum difference of 8% between the two TDs. These differences can be well explained by differences in the residence times in the heating sections of the two TD designs.

Fig. 10 shows the normalized size distributions of NaCl particles coated with DEHS, before and after heating. The curve "NaCl only" refers to the size distribution of the monodisperse aerosol particles before entering the Erlenmeyer containing DEHS. The size distribution of NaCl coated particles at 25 °C is that of the aerosol entering the VDMA system (cf. Fig. 6).

The measurements shown in Fig. 10a (obtained at 25 °C), suggest that coating was successfully accomplished, since most NaCl particles grew substantially, exceeding the maximum observed size of 125 nm while the size distribution of the resulting aerosol became significantly wide. The widespread size distribution of coated particles can be attributed to the vast range of residence times of NaCl particles in the Erlenmeyer flask, resulting in a very broad distribution of condensate DEHS onto the NaCl particles. When the temperature in the TD increased to 80 °C (cf. Fig. 10b) it was already possible to observe a partial recovery of NaCl particles to their original size, whereas at 120 °C (cf. c) the original size distribution was completely recovered, indicating that all DEHS was volatilized.

Similarly to the case with ammonium sulphate, the cTD evaporated a higher fraction of organic species from the coated particles in comparison with the NanoTD at intermediate temperatures, probably due to the lower residence time in the heating section of the later.

Fig. 11 shows the fraction of NaCl particles that were stripped from DEHS until the original size was recovered. Any NaCl particles with final sizes that fall into the "NaCl-only" size distribution is considered as totally free of DEHS. To investigate the influence of the initial particle size on the results, monodisperse NaCl particles having diameters of 50 and 100 nm were used.

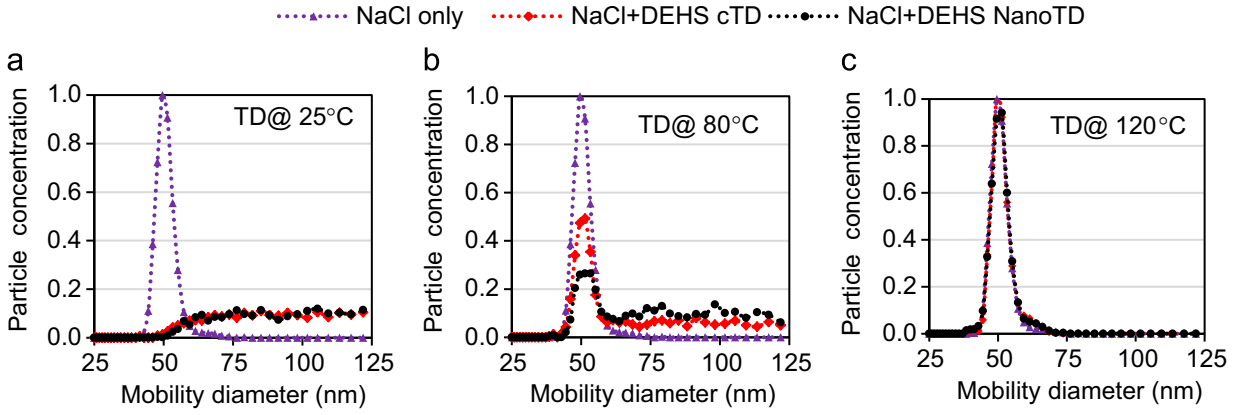

Fig. 10. Volatility of 50-nm NaCl particles coated with DEHS for TD operation temperatures of (a) 25 °C, (b) 80 °C and (c) 120 °C. The particle number concentration was normalized.

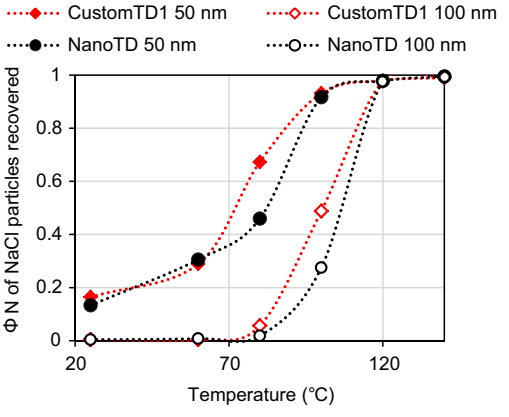

Fig. 11. NaCl particles recovery after DEHS volatilization. The lines with filled markers refer to NaCl particles with initial size of 50 nm, and the open markers to an initial size of 100 nm.

It becomes clear that larger particles require higher temperatures to vaporize the volatile species. Larger particles have higher enthalpy, requiring larger amount of energy to heat them to a certain temperature. Furthermore, 100-nm particles, due to their higher surface area, have the ability to carry more DEHS, resulting in higher volatile fraction load into the system, as well as the enhancement of the already higher enthalpy.

The performance differences between TD designs are mainly noticed when the volatilization rate, i.e., the ratio between changes in aerosol fractions ($\Delta\Phi$) and the applied temperature (ΔT), is high. The volatilization rate was enhanced in the temperature ranges 60–100 °C and 80–120 °C, for 50- and 100-nm particles, respectively. At the highest volatilization rates we also observed a difference of about 21% in the performance between the two TDs, which is not dependent on particle size. It must be noted here that the volatile fraction loads used in these experiments were generally beyond the loads found in regular outdoor/indoor environments.

3.2.2. Ambient aerosol tests

While laboratory-generated aerosol particles have a known composition, the ambient aerosol is a complex mixture of myriad of components, which makes their behavior difficult to predict.

Fig. 12 compares VTDMA measurements of urban background aerosol samples using the two TDs. ΦN remains nearly constant for 80- and 150-nm particles, indicating that most particles partially consist of non-volatile species. The decreasing ΦN for particles with Dp_{in} of 30 and 50 nm may be caused by particle shrinkage to a size smaller than the detection limit level (DLL) of DMA-2 and CPC, which in this specific experiment is 13 nm, or by the complete volatilization of the sampled particles. The results shown in Fig. 13, corresponding to 50-nm particles, strongly suggest that particles smaller than the DLL are the main cause of the sudden decrease in ΦN, since the mode of the measured distribution is clearly extended to sizes that are not detectable by our system. Both TDs exhibited a similar trend in ΦN, but the cTD showed constantly lower remaining number fraction. This difference is barely noticeable for 150-nm particles, which did not shrink to sizes smaller than the DLL even at 230 °C. ΦV represents a sensitive variable for expressing particle shrinkage, and is therefore suitable for comparing the performance of different TDs.

The NanoTD unit achieved similar volatilization rates with the cTD when the particle shrinkage rate was low. This happened when temperature was too low to volatilize any compounds, or too high and the volatilization was completed. However, at intermediate temperatures that lead to high volatilization rate, given by the slope of the $\Phi V(T)$ curve, the NanoTD unit achieved lower particle volatilization, with a maximum difference of 12% in the remaining particles volume.

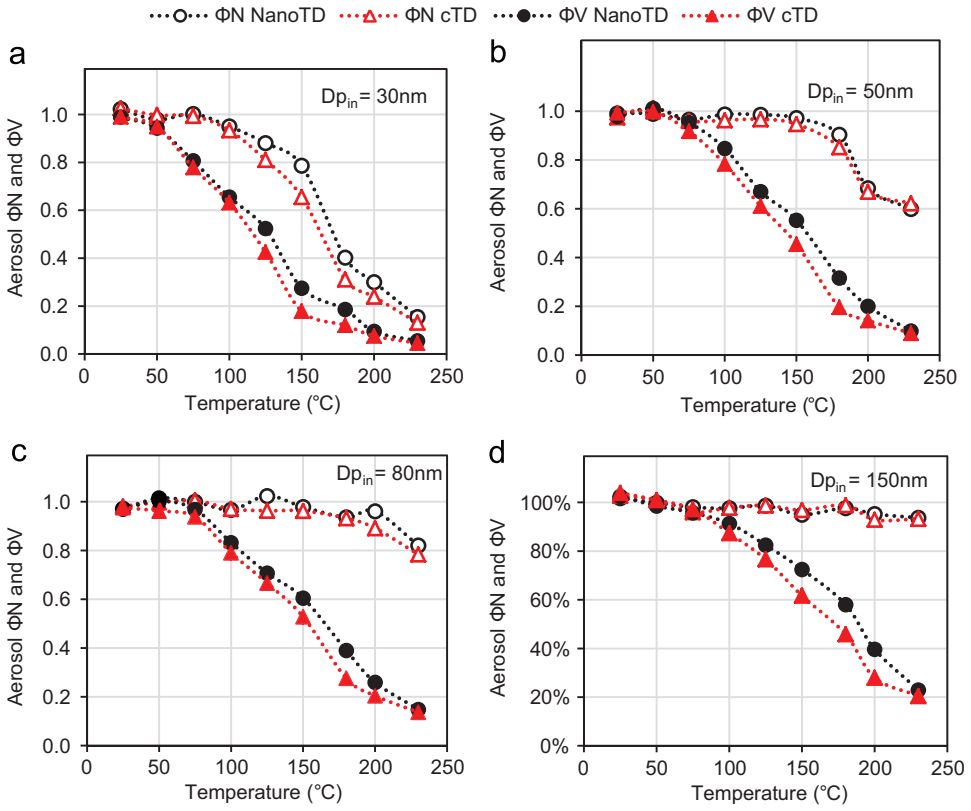

Fig. 12. Ambient aerosol volatility at the urban background station for particles with dry sizes of (a) 30 nm, (b) 50 nm, (c) 80 nm and (d) 150 nm. Filled and open markers represent the volume and number fractions remaining, respectively.

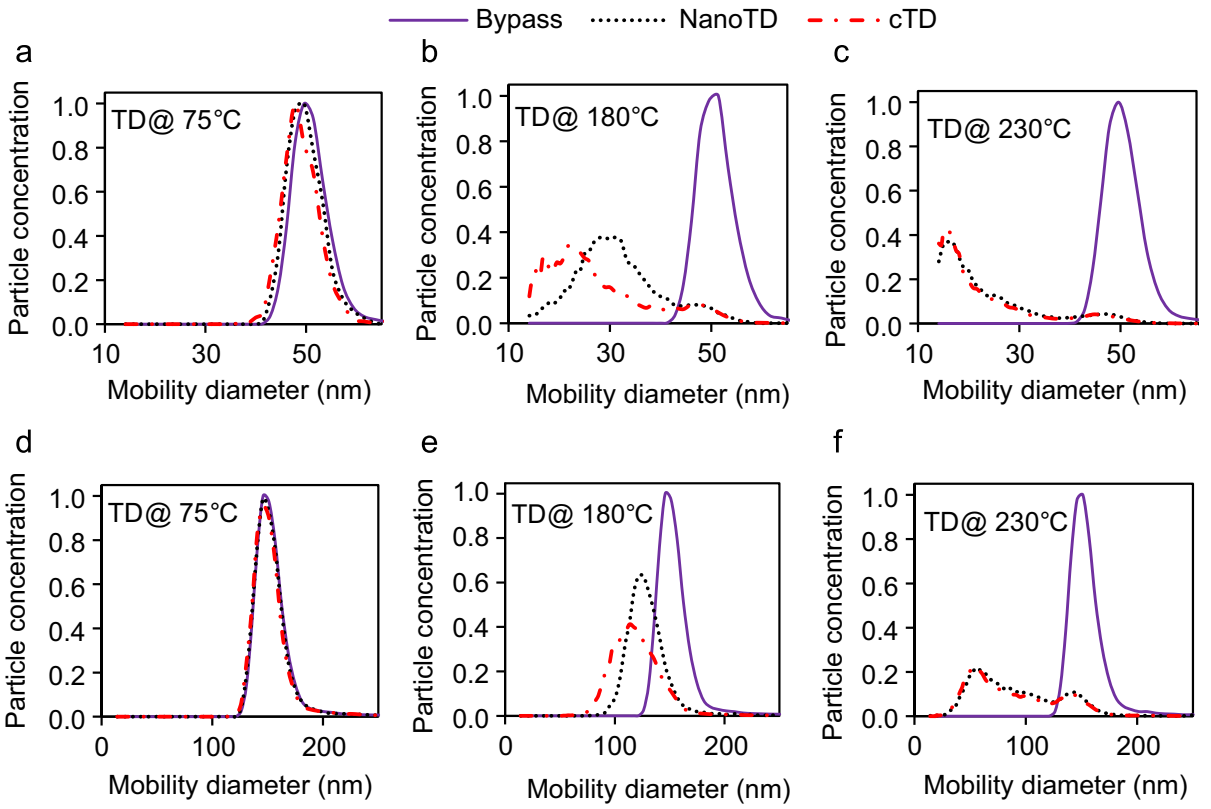

Fig. 13. Number size distributions of 50-nm particles after heating at (a) 75 °C, (b) 180 °C and (c) 230 °C, and 150-nm particles after heating at (d) 75 °C, (e) 180 °C and (f) 230 °C. All particle number concentrations were normalized.

This difference was rather stable among the particle sizes analyzed, ranging between 9 and 12%. However, the temperature at which these maxima were achieved increased with particle size, being 150 °C for 30-nm and between 180 and 200 °C for 150-nm particles. This behavior can be the result of the higher enthalpy of the larger particles, or different chemical compositions between particle sizes.

The volatilization rate was greatly reduced in the temperature range 200–230 °C, indicating that the particles studied here approached their final volatilization stage. This result supports the idea that most ambient aerosol volatile species have evaporated at 300 °C, with only the refractory fraction remaining. Fig. 13 shows the average particle size distributions of 50- and 150-nm particles sampled from urban background aerosols, after conditioning at 75, 180 and 230 °C, matching the data shown in Fig. 12b and d. Comparison between the distributions shown in these figures reflects the correlation between changes in ΦV and ΦN with particle size.

The 30-nm particles shown a slight shift in size at 75 °C, while at 180 °C the size distribution was bimodal, with the more volatile particles shrinking to sizes smaller than the DLL, yielding the particle number reduction shown by the data in Fig. 12b. At 230 °C, this effect was even more pronounced and the volatilization difference between TDs was negligible.

For 150-nm particles exposed at 75 °C, there was no change in particle size or number. At 180 °C both TDs yielded a unimodal size distribution, shifted to smaller sizes, indicating partial particle volume loss. The size distribution resulting from the cTD showed a wider mode with mean particle size about 10 nm smaller than that from the NanoTD, which represents a 12% difference in ΦV. At 230 °C the differences between TDs were negligible. At this temperature, both TDs yielded a similar bimodal size distribution, with one mode corresponding to fully non-volatile particles and the other mode corresponding to partially volatile particles. The remaining unchanged number fraction indicates the presence of a solid non-volatile core in all particles for the urban background aerosol samples studied here. This is observed in the measurements using both TDs and clarifies the ability of the VTDMA system to separate particle populations according to their volatility.

4. Conclusions

In this paper we characterize and evaluate the overall performance of two thermodenuders (a NanoTD described by Fierz et al. (2007), and a custom-made coiled TD) using VTDMA measurements. The NanoTD is a straight tube with shorter aerosol residence time (1 s at 25 °C and 0.3 L min^{-1}), providing low diffusional and thermophoretic loses. This makes the NanoTD suitable for UFP analysis, even at low particle concentrations. The *c*TD is a longer coiled tube with a passively cooled adsorption section. The *c*TD allows higher residence times (3.2 s at 25 °C and 0.3 L min^{-1}) and operating temperatures in a compact design. However, the design of this TD exhibits higher diffusional and thermophoretic particle losses. The overall losses in the *c*TD increase on average by 8% at 300 °C, relative to those measured at ambient temperature. These results were successfully validated by two thermophoretic deposition models using fluid and heat transfer simulations to determine flow and temperature profiles.

The maximum difference in remaining volume fraction of ammonium sulphate particles using the two TDs was 20% at 180 °C. When volatilizing core–shell NaCl particles coated with DEHS, the difference in the number of particles from which DEHS was completely evaporated between the two TD designs exhibited a maximum of 21%, independently of the size of NaCl particles. Nonetheless, the temperature at which this maximum was achieved increased with particle size as a result of the higher enthalpy of the larger particles. For ambient aerosols, the differences in the measured remaining particle volume between the two TD designs had a maximum value of 9% for 30-nm particles at 150 °C and 12% for 150-nm particles at 200 °C. The difference between TDs is only noticeable at temperatures at which the volatilization rate is higher, and varies depending on aerosol composition. The findings of our study suggest that direct comparison between volatility measurements using different TDs must be carefully analyzed, and always accompanied by a detailed description of the TD and the operating conditions used.

Acknowledgments

The present study was supported by the European Union Seventh Framework Programme (FP7/2007-2013) under Grant agreement no. 315760: Marie Curie ITN project HEXACOMM.

Our thanks are due to Dr. Ian Cobeck, University of Essex, for providing major components of the VTDMA system.

References

An, W. J., Pathak, R. K., Lee, B.-H., & Pandis, S. N. (2007). Aerosol volatility measurement using an improved thermodenuder: Application to secondary organic aerosol. *Journal of Aerosol Science*, *38*, 305–314, http://dx.doi.org/10.1016/j.jaerosci.2006.12.002.

Batchelor, G. K., & Shen, C. (1985). Thermophoretic deposition of particles in gas flowing over cold surfaces. *Journal of Colloid and Interface Science 107*, 21–37.

Bezantakos, S., Huang, L., Barmpounis, K., Attoui, M., Schmidt-Ott, A., & Biskos, G. (2015). A cost-effective electrostatic precipitator for aerosol nanoparticle segregation. *Aerosol Science and Technology*, *49*, iv–vi, http://dx.doi.org/10.1080/02786826.2014.1002829.

Birmili, W., Heinke, K., Pitz, M., Matschullat, J., Wiedensohler, A., Cyrys, J., et al. (2010). Particle number size distributions in urban air before and after volatilisation. *Atmospheric Chemistry and Physics*, *10*, 4643–4660, http://dx.doi.org/10.5194/acp-10-4643-2010.

Brooks, B. J., Smith, M. H., Hill, M. K., & O'Dowd, C. D. (2002). Size-differentiated volatility analysis of internally mixed laboratory-generated aerosol. *Journal of Aerosol Science*, *33*, 555–579.

Burtscher, H., Baltensperger, U., Bukowiecki, N., Cohn, P., Hu, C., Mohr, M., et al.(2001). *Separation of volatile and non-volatile aerosol fractions by thermodesorption: instrumental development and applications* (Vol. 32, pp. 427–442).

Cappa, C. D. (2010). A model of aerosol evaporation kinetics in a thermodenuder. *Atmospheric Measurement Techniques*, *3*, 579–592, http://dx.doi.org/10.5194/amt-3-579-2010.

Colome, S. D., Kado, N. Y., Jaques, P., & Kleinman, M. (1992). Indoor–outdoor air pollution relations: particulate matter less than 10 μm in aerodynamic diameter (PM10) in homes of asthmatics. *Atmospheric Environment Part A General Topics*http://dx.doi.org/10.1016/0960-1686(92)90405-A.

Cubison, M. J., Coe, H., & Gysel, M. (2005). A modified hygroscopic tandem DMA and a data retrieval method based on optimal estimation. *Journal of Aerosol Science*, *36*, 846–865, http://dx.doi.org/10.1016/j.jaerosci.2004.11.009.

Cullen, R. T., Tran, C. L., Buchanan, D., Davis, J. M., Searl, A., Jones, A. D., et al. (2000). Inhalation of poorly soluble particles. I. Differences in inflammatory response and clearance during exposure. *Inhalation Toxicology*, *12*, 1089–1111, http://dx.doi.org/10.1080/08958370050166787.

Davidson, C. I., Phalen, R. F., & Solomon, P. A. (2005). Airborne particulate matter and human health: A review. *Aerosol Science and Technology*http://dx.doi.org/10.1080/02786820500191348.

Donaldson, K., Brown, D., Clouter, A., Duffin, R., MacNee, W., Renwick, L., et al. (2002). The pulmonary toxicology of ultrafine particles. *Journal of Aerosol Medicine*, *15*, 213–220, http://dx.doi.org/10.1089/089426802320282338.

Engler, C., Rose, D., Wehner, B., Wiedensohler, A., Brüggemann, E., Gnauk, T., et al. (2007). Size distributions of non-volatile particle residuals ($D_p < 800$ nm) at a rural site in Germany and relation to air mass origin. *Atmospheric Chemistry and Physics*, *7*, 5785–5802, http://dx.doi.org/10.5194/acp-7-5785-2007.

Faulhaber, A. E., Thomas, B. M., Jimenez, J. L., Jayne, J. T., Worsnop, D. R., & Ziemann, P. J. (2009). Characterization of a thermodenuder-particle beam mass spectrometer system for the study of organic aerosol volatility and composition. *Atmospheric Measurement Techniques*http://dx.doi.org/10.5194/amt-2-15-2009.

Fierz, M., Vernooij, M. G. C., & Burtscher, H. (2007). An improved low-flow thermodenuder*Journal of Aerosol Science*, *38*, 1163–1168, http://dx.doi.org/10.1016/j.jaerosci.2007.08.006.

Frey, A., Rose, D., Wehner, B., Müller, T., Cheng, Y., Wiedensohler, A., et al. (2008). Application of the volatility-TDMA technique to determine the number size distribution and mass concentration of less volatile particles. *Aerosol Science and Technology*http://dx.doi.org/10.1080/02786820802339595.

Gysel, M., Mcfiggans, G. B., & Coe, H. (2009). Inversion of tandem differential mobility analyser (TDMA) measurements*Journal of Aerosol Science*, *40*, 134–151 , http://dx.doi.org/10.1016/j.jaerosci.2008.07.013.

Harrison, R. M., & Yin, J. (2000). Particulate matter in the atmosphere: Which particle properties are important for its effects on health?. *Science of the Total Environment*http://dx.doi.org/10.1016/S0048-9697(99)00513-6.

Hinds, W. C. (1999). *Aerosol technology* 2nd ed.). New York: Wiley.

Housiadas, C., & Drossinos, Y. (2005). Thermophoretic deposition in tube flow. *Aerosol Science and Technology.*, *39*, 304–318, http://dx.doi.org/10.1080/027868290931069.
Huffman, J. A., Docherty, K. S., Aiken, A. C., Cubison, M. J., Ulbrich, I. M., et al. (2009). Chemically-resolved aerosol volatility measurements from two megacity field studies*Atmospheric Chemistry and Physics Discussions*, 7161–7182.
ICRP. (1995). ICRP publication 66: Human respiratory tract model for radiological protection. *Annals of ICRP*, *24*http://dx.doi.org/10.1016/0146-6453(94)90029-9.
IPCC, I. P. O. C. C. (2007). Climate change 2007—The physical science basis: Working group I contribution to the fourth assessment report of the IPCC. *Science80*, 1009.
Jennings, S. G., O'Dowd, C. D., Cooke, W. F., Sheridan, P. J., & Cachier, H. (1994). Volatility of elemental carbon. *Geophysical Research Letters*http://dx.doi.org/10.1029/94GL01423.
Johnson, G. R., Ristovski, Z., & Morawska, L. (2004). Method for measuring the hygroscopic behaviour of lower volatility fractions in an internally mixed aerosol. *Journal of Aerosol Science*, *35*, 443–455, http://dx.doi.org/10.1016/j.jaerosci.2003.10.008.
Jokinen, V., & Mfikelfi, J. M. (1997). Closed-loop arrangement with critical orifice for dma sheath/excess flow system*Journal of Aerosol Science*, *28*, 643–648.
Karnezi, E., Riipinen, I., & Pandis, S. N. (2014). Measuring the atmospheric organic aerosol volatility distribution: A theoretical analysis. *Atmospheric Measurement Techniques*, *7*, 2953–2965, http://dx.doi.org/10.5194/amt-7-2953-2014.
Kawanaka, Y., Matsumoto, E., Sakamoto, K., & Yun, S. J. (2011). Estimation of the contribution of ultrafine particles to lung deposition of particle-bound mutagens in the atmosphere. *Science of the Total Environment.*, *409*, 1033–1038, http://dx.doi.org/10.1016/j.scitotenv.2010.11.035.
Kuhn, T., Biswas, S., Fine, P. M., Geller, M., & Sioutas, C. (2005). Physical and chemical characteristics and volatility of PM in the proximity of a light-duty vehicle freeway. *Aerosol Science and Technology*, *39*, 347–357, http://dx.doi.org/10.1080/027868290930024.
Kuhn, T., Biswas, S., & Sioutas, C. (2005). Diurnal and seasonal characteristics of particle volatility and chemical composition in the vicinity of a light-duty vehicle freeway. *Atmospheric Environment*, *39*, 7154–7166, http://dx.doi.org/10.1016/j.atmosenv.2005.08.025.
Kuhn, T., Krudysz, M., Zhu, Y., Fine, P. M., Hinds, W. C., Froines, J., et al. (2005). Volatility of indoor and outdoor ultrafine particulate matter near a freeway*Journal of Aerosol Science*, *36*, 291–302, http://dx.doi.org/10.1016/j.jaerosci.2004.09.006.
Li, N., Sioutas, C., Cho, A., Schmitz, D., Misra, C., Sempf, J., et al. (2003). Ultrafine particulate pollutants induce oxidative stress and mitochondrial damage. *Environmental Health Perspectives*, *111*, 455–460, http://dx.doi.org/10.1289/ehp.6000.
Lin, J.-S., & Tsai, C.-J. (2003). Thermophoretic deposition efficiency in a cylindrical tube taking into account developing flow at the entrance region. *Journal of Aerosol Science*, *34*, 569–583, http://dx.doi.org/10.1016/S0021-8502(03)00023-5.
Liu, B. Y. H., Pui, D. Y. H., Whitby, K. T., Kittelson, D. B., Kousaka, Y., & McKenzie, R. L. (1978). The aerosol mobility chromatograph: A new detector for sulfuric acid aerosols. *Atmospheric Environment*, *12*, 99–104, http://dx.doi.org/10.1016/0004-6981(78)90192-0.
Lohmann, U., & Feichter, J. (2004). Global indirect aerosol effects: A review. *Atmospheric Chemistry and Physics Discussion*http://dx.doi.org/10.5194/acpd-4-7561-2004.
MacNee, W., & Donaldson, K. (2003). Mechanism of lung injury caused by PM10 and ultrafine particles with special reference to COPD. *European Respiratory Journal. Supplement*, *40*, 47s–51s, http://dx.doi.org/10.1183/09031936.03.00403203.
Maruf Hossain, A. M., Park, S., Kim, J. S., & Park, K. (2012). Volatility and mixing states of ultrafine particles from biomass burning. *Journal of Hazardous Materials*http://dx.doi.org/10.1016/j.jhazmat.2011.12.061.
Moore, K. F., Ning, Z., Ntziachristos, L., Schauer, J. J., & Sioutas, C. (2007). Daily variation in the properties of urban ultrafine aerosol—Part I: Physical characterization and volatility. *Atmospheric Environment*, *41*, 8633–8646, http://dx.doi.org/10.1016/j.atmosenv.2007.07.030.
Nyeki, S., Coulson, G., & Colbeck, I. (2005). Overview of aerosol microphysics at Arctic sunrise: Measurements during the NICE renoxification study. *Tellus B*, *2001*, 40–50.
O'Dowd, C. D., Jennings, S. G., Smith, M. H., & Cooke, W. (1992). A high temperature volatility technique for determination of atmospheric aerosol composition. *Journal of Aerosol Science*, *23*, 905–908, http://dx.doi.org/10.1016/0021-8502(92)90558-D.
Oberdörster, G., Sharp, Z., Atudorei, V., Elder, A., Gelein, R., Kreyling, W., & Cox, C. (2004). Translocation of inhaled ultrafine particles to the brain. *Inhalation Toxicology*, *16*, 437–445, http://dx.doi.org/10.1080/08958370490439597.
Orsini, D. A., Wiedensohler, A., Stratmann, F., Covert, D. S., Atmospheric, J. O. F., & Technology, O. (1999). A new volatility tandem differential mobility analyzer to measure the volatile sulfuric acid aerosol fraction. *Journal of Atmospheric and Oceanic Technology*, *16*, 760–772, http://dx.doi.org/10.1175/1520-0426(1999)016<0760:ANVTDM>2.0.CO;2.
Paulsen, D., Weingartner, E., Rami Alfarra, M., & Baltensperger, U. (2006). Volatility measurements of photochemically and nebulizer-generated organic aerosol particles. *Journal of Aerosol Science*, *37*, 1025–1051, http://dx.doi.org/10.1016/j.jaerosci.2005.08.004.
Philippin, S., Wiedensohler, A., & Stratmann, F. (2004). Measurements of non-volatile fractions of pollution aerosols with an eight-tube volatility tandem di erential mobility analyzer (VTDMA-8)*Journal of Aerosol Science*, *35*, 185–203, http://dx.doi.org/10.1016/j.jaerosci.2003.07.004.
Pope, C. A. (2000). Epidemiology of fine particulate air pollution and human health: Biologic mechanisms and who's at risk?. *Environmental Health Perspectives*, *108*, 713–723, http://dx.doi.org/10.1289/ehp.00108s4713.
Poulain, L., Birmili, W., Canonaco, F., Crippa, M., Wu, Z. J., Nordmann, S., et al. (2014). Chemical mass balance of 300 °C non-volatile particles at the tropospheric research site Melpitz, Germany. *Atmospheric Chemistry and Physics*, *14*, 10145–10162, http://dx.doi.org/10.5194/acp-14-10145-2014.
Rader, D. J., & McMurry, P. H. (1986). Application of the tandem differential mobility analyzer to studies of droplet growth or evaporation. *Journal of Aerosol Science*http://dx.doi.org/10.1016/0021-8502(86)90031-5.
Riipinen, I., Pierce, J. R., Donahue, N. M., & Pandis, S. N. (2010). Equilibration time scales of organic aerosol inside thermodenuders: Evaporation kinetics versus thermodynamics. *Atmospheric Environment*, *44*, 597–607, http://dx.doi.org/10.1016/j.atmosenv.2009.11.022.
Romay, F. J., Takagaki, S. S., Pui, D. Y. H., & Liu, B. Y. H. (1998). Thermophoretic deposition of aerosol particles in turbulent pipe flow. *Journal of Aerosol Science*, *29*, 943–959, http://dx.doi.org/10.1016/S0021-8502(98)00004-4.
Sakurai, H., Park, K., Mcmurry, P. H., & Kittelson, D. B. (2003). Size-dependent mixing characteristics of volatile and nonvolatile components in diesel exhaust aerosols*Environmental Science & Technology*, *37*, 5487–5495.
Saleh, R., Shihadeh, A., & Khlystov, A. (2011). On transport phenomena and equilibration time scales in thermodenuders*Atmospheric Measurement Techniques*, 571–581, http://dx.doi.org/10.5194/amt-4-571-2011.
Stolzenburg, M. R., & McMurry, P. H. (2008). Equations governing single and tandem DMA configurations and a new lognormal approximation to the transfer function. *Aerosol Science and Technology.*, *42*, 421–432, http://dx.doi.org/10.1080/02786820802157823.
Stratmann, F., Otto, E., & Fissan, H. (1994). Thermophoretical and diffusional particle transport in cooled laminar tube flow. *Journal of Aerosol Science*, *25*, 1305–1319.
Talbot, L., Cheng, R. K., Schefer, R. W., & Willis, D. R. (1980). Thermophoresis of particles in a heated boundary layer. *Journal of Fluid Mechanics.*
Taylor, P. (2007). Design and validation of a 6-volatility tandem differential mobility analyzer (VTDMA)*Aerosol Science and Technology*http://dx.doi.org/10.1080/02786820701534593.
Tiitta, P., Miettinen, P., Vaattovaara, P., Joutsensaari, J., Peta, T., et al. (2010). Roadside aerosol study using hygroscopic, organic and volatility TDMAs. *Characterization and mixing state*, *44*, 976–986, http://dx.doi.org/10.1016/j.atmosenv.2009.06.021.
Villani, P., Picard, D., Marchand, N., & Laj, P. (2007). Design and validation of a 6-volatility tandem differential mobility analyzer (VTDMA). *Aerosol Science and Technology.*
Von Klot, S., Peters, A., Aalto, P., Bellander, T., Berglind, N., et al. (2005). Ambient air pollution is associated with increased risk of hospital cardiac readmissions of myocardial infarction survivors in five European cities. *Circulation*, *112*, 3073–3079, http://dx.doi.org/10.1161/CIRCULATIONAHA.105.548743.
Walker, K. L., Homsy, G. M., & Geyling, F. T. (1979). Thermophoretic deposition of small particles in laminar tube flow. *Journal of Colloid and Interface Science*, *69*, 138–147, http://dx.doi.org/10.1016/0021-9797(79)90088-2.

Walsh, J. K., Weimer, a W., & Hrenya, C. M. (2006). Thermophoretic deposition of aerosol particles in laminar tube flow with mixed convection. *Journal of Aerosol Science*, *37*, 715–734, http://dx.doi.org/10.1016/j.jaerosci.2005.05.017.

Wehner, B., Philippin, S., Wiedensohler, A., Scheer, V., & Vogt, R. (2004). Variability of non-volatile fractions of atmospheric aerosol particles with traffic influence. *Atmospheric Environment*, *38*, 6081–6090, http://dx.doi.org/10.1016/j.atmosenv.2004.08.015.

Yook, S.-J., & Pui, D. Y. H. (2006). Experimental study of nanoparticle penetration efficiency through coils of circular cross-sections. *Aerosol Science and Technology.*, *40*, 456–462, http://dx.doi.org/10.1080/02786820600660895.